Submitted for Publication to Journal of Fluids Engineering
ASME Transactions
ACCEPTED FOR PUBLICATION, FINAL VERSION
10/8/2007

Effect of Surface Roughness on Single Cryogen Droplet Spreading

Jie Liu
e-mail: liuj@engr.ucr.edu
Department of Mechanical Engineering,
University of California, Riverside CA 92521

Walfre Franco
email: wfranco@uci.edu
Beckman Laser Institute and Medical Clinic,
University of California, Irvine
1002 Health Sciences Road East,
Irvine, CA 92612

Guillermo Aguilar
e-mail: gaguilar@engr.ucr.edu
Department of Mechanical Engineering,
University of California, Riverside CA 92521

Abstract

Cryogen spray cooling (CSC) is an auxiliary procedure to dermatologic laser surgery which consists of pre-cooling the superficial skin layer (epidermis) during laser irradiation of subsurface targets to avoid non-specific epidermal thermal damage. While previous studies have investigated the interaction of cryogen sprays with microscopically smooth human skin models, it is important to recognize that real human skin surface is far from smooth. With the objective to provide physical insight into the interaction between cryogen sprays and human skin, we study the effect of surface roughness on the impact dynamics of single cryogen droplets falling on skin models of various roughnesses (0.5 μm to 70 μm). We first develop a theoretical model to predict the maximum spread diameter (D_m) following droplet impingement based on a similarity approximation to the solution of a viscous boundary-layer that incorporates friction as the major source of viscous dissipation on a rough surface. Then, we measure droplet

diameter, impact velocity and D_m of cryogen droplets falling by gravity onto skin models. Experimental data prove that the proposed model predicts D_m with good accuracy, suggesting that the effects of surface roughness and friction on D_m are properly taken into account for the range of surface roughness studied herein.

1. Introduction

Dermatological laser surgery is the treatment of choice for vascular lesions (e.g., hemangiomas [1] and Port Wine Stain (PWS) birthmarks [2]) as well as cosmetic surgery (e.g., hair [3] and tattoo [4] removal). In these treatments, cryogen spray cooling (CSC) is an essential auxiliary method that protects the epidermis from excessive thermal damage during laser irradiation, while subdermic targets, such as PWS blood vessels located 100–500 μm below the skin surface [5], are thermally photocoagulated. The only FDA-approved cryogen used thus far for this purpose is Tetrafluoroethane-1,1,1,2 (R134a) [3], with a boiling temperature of -26 ^{o}C at atmospheric pressure. Short cryogen spurts (20–100 ms) [6, 7] are released from a pressurized container through a spray valve/nozzle system. Well-atomized cryogen droplets with diameters of 3–20 μm [8] and velocities 10–80 m/s [9, 10] impact onto human skin and extract heat as they spread and evaporate.

The efficiency of heat extraction during spray deposition is largely dictated by the dynamics of droplet impact [8]. Ideally, micrometer-size cryogen droplets impact and spread on the skin surface evaporating and extracting heat. Previous studies [5, 11-13] used epoxy resins or Plexiglas substrates as skin models to measure the heat extraction induced by short cryogen spurts. These studies concluded that the thickness of the cryogen layer on the skin surface influences greatly the heat transfer during CSC. The

skin models used in these studies were macroscopically smooth; however, the human skin surface is far from smooth. Moreover, human skin roughness varies with age, anatomical location and environmental factors such as sun exposure and humidity [14].

In this present study, we first use a simple but realistic experimental scenario where the liquid layer (formed by the coalescence of thousands or millions of droplets) that spreads on the human skin surface is represented and indirectly measured by the maximum spread diameter (D_m) of a single droplet [6]. This scenario allows us to maintain proper scaling while significantly simplifying the more complex spray problem. In this study, we investigate the dynamics of single droplet impact onto flat rigid surfaces with surface roughnesses (Ra) in the range of 0.5 to 70 μm, which include those characteristic of human skin: 50-200 μm. Subsequently, we use these experimental results to develop a new semi-empirical model to predict D_m without considering evaporation. Finally, we use discrete experimental data to obtain the free parameters required by our model and compare its predictions to those of previous models and to a comprehensive experimental data set.

2. History of numerical models

Figure 1 shows a schematic of the droplet geometry before and after impact on a flat surface and the associated mass and energy conservation equations. Before impact, the geometry of the droplet is close to a perfect sphere of diameter D moving with velocity V. The total energy of the droplet at this stage E_1 can be expressed as [15]:

$$E_1 = \left(\frac{1}{2}\rho V^2\right)\left(\frac{1}{6}\pi D\right)^3 + \pi D^2 \sigma_{LV}\,, \tag{1}$$

where the two terms on the right represent kinetic energy and surface energy of the droplet, respectively.

After impact, the cryogen droplet spreads along the surface until it reaches the maximum spread diameter, D_m. At this stage, the geometry of the cryogen can be modeled as a disc of diameter D_m and thickness h, where $h = \frac{2D^3}{3D_m^2}$ according to mass conservation. Since the kinetic energy of the droplet reduces to zero at maximum spreading, the total energy of the flattened droplet only consists of the surface energy [15]:

$$E_2 = \left(\frac{\pi}{4} D_m^2 + \frac{2}{3} \pi \frac{D^3}{D_m} \right) \sigma_{LV} + \frac{\pi}{4} D_m^2 \left(\sigma_{SL} - \sigma_{SV} \right). \tag{2}$$

The first term on the right of Eq. 2 represents the surface energy between the liquid and vapor at the top and peripheral areas of the flattened liquid droplet, while the second term represents the surface energy of the droplet. The three surface tensions (σ_{LV}, σ_{SL}, and σ_{SV}) are related to each other through the static contact angle θ [16]:

$$\sigma_{LV} \cos\theta = \sigma_{SL} - \sigma_{SV} . \tag{3}$$

Substituting Eq. (3) into (2), the total energy at this stage can be rewritten as:

$$E_2 = \left[\frac{\pi}{4} D_m^2 \left(1 - \cos\theta\right) + \frac{2}{3} \pi \frac{D^3}{D_m} \right] \sigma_{LV} . \tag{4}$$

According to energy conservation, Eq. (1) must be written as

$$\left(\frac{1}{2} \rho V^2 \right) \left(\frac{1}{6} \pi D^3 \right) + \pi D^2 \sigma_{LV} = \left[\frac{\pi}{4} D_m^2 (1 - \cos\theta) + \frac{2}{3} \pi \frac{D^3}{D_m} \right] \sigma_{LV} + W_{Diss} , \tag{5}$$

Where W_{Diss} is the energy dissipation during the spread process. Several papers have discussed how to evaluate this term. Chandra *et al.* [15] suggested that W_{Diss} could be solved using the following approximation:

$$W_{Diss} = \int_0^{t_c} \int_\Omega \phi d\Omega dt \approx \phi \Omega t_c \,, \tag{6}$$

where ϕ, the dissipation function, is defined as:

$$\phi = \eta \left(\frac{V}{h} \right)^2 , \tag{7}$$

η is the dynamic viscosity and Ω is the liquid droplet volume, which once the droplet reaches D_m is defined as:

$$\Omega = \frac{1}{4} \pi D_m^2 h \,, \tag{8}$$

and t_c is the characteristic time from droplet impact to maximum spread, simply defined as [15]:

$$t_c \approx D / V \,. \tag{9}$$

Combining Eq. (6)–(9) yields

$$W_{Diss} = \frac{1}{4} \pi \eta (V / h) D D_m^2 \,. \tag{10}$$

Inserting Eq. (10) into Eq. (5), and applying the definitions of Reynolds and Weber numbers ($Re = \rho DV/\eta$ and $We = \rho DV^2/\sigma$, where ρ is the density, D is the droplet diameter, V is the impact velocity， η is cryogen viscosity and σ is the surface tension), the energy equation becomes

$$\frac{3}{2} \frac{We}{Re} \beta^4 + (1 - cos\,\theta) \beta^2 - \left(\frac{1}{3} We + 4 \right) = 0 \,, \tag{11}$$

where $\beta = D_m/D$ is the normalized maximum spread diameter. To get more accurate results, Pasandideh-Fard *et al.* [17] considered droplet spreading as an axi-symmetric stagnation flow and used it to find W_{Diss} as follows. In cylindrical coordinates, the simplified continuity equation becomes:

$$\frac{V_r}{r} + \frac{\partial V_r}{\partial r} + \frac{\partial V_z}{\partial z} = 0\,, \tag{12}$$

and the Navies-Stokes equation in the radial direction (r) becomes:

$$\frac{\partial V_r}{\partial t} + V_r \frac{\partial V_r}{\partial r} + V_r \frac{\partial V_z}{\partial z} = -\frac{1}{\rho}\frac{\partial P}{\partial r} + \nu\left[\frac{\partial^2 V_r}{\partial r^2} + \frac{1}{r}\frac{\partial V_r}{\partial r} + \frac{\partial^2 V_r}{\partial z^2} - \frac{V_r}{r^2}\right]. \tag{13}$$

For a steady state axi-symmetric stagnation flow, the similarity method can be used to find the thickness of boundary layer δ. This method requires the introduction of a stream function ψ that satisfies the no-slip condition, a similarity variable α, and a similarity function $G'(\alpha)$ defined as

$$\psi = -Br^2 z \qquad \alpha = z\sqrt{\frac{B}{\nu}} \qquad G'(\alpha) = \frac{V_r}{Br} \tag{14}$$

where B is a constant parameter with units of 1/sec that must be defined. In terms of ψ, the radial component of the velocity V_r may be expressed as:

$$V_r = -\frac{1}{r}\frac{\partial \psi}{\partial z} = Br\,. \tag{15}$$

$G'(\alpha)$ represents a dimensionless velocity, which takes a value of ~ 1 when α = 2.4. Thus the thickness of the boundary layer of an axi-symmetric stagnation flow can be obtained [18] using Eq. (14). Pasandideh-Fard *et al.* [17] proposed the spread velocity V_r to be equal to the impingement velocity V ($V_r = V$) and assumed $B = V/D$. In this case δ becomes

$$\delta = \frac{2.4D}{\sqrt{Re}}, \tag{16}$$

and ϕ in (6) becomes

$$\phi \approx \eta\left(\frac{V}{\delta}\right)^2, \tag{17}$$

which differs from Eq. 7 since h is replaced by δ. Another significant difference from the model of Chandra *et al.* [15] is the definition of t_c, which Pasandideh-Fard *et al.* defined as

$$t_c = \frac{8}{3}\frac{D}{V}. \tag{18}$$

By combining Eqs. (5), (6) and (16)–(18), Pasandideh-Fard *et al.* obtained

$$4\frac{We}{\sqrt{\mathrm{Re}}}\beta^3 + 3(1-\cos\theta)\beta^2 - (We+12) = 0. \tag{19}$$

Mao *et al.* [19] subsequently modified the above equation according to experimental results and obtained

$$0.2\frac{We^{0.83}}{Re^{0.33}}\beta^3 + \frac{1}{4}(1-cos\,\theta)\beta^2 - \left(\frac{We}{12}+1\right)\beta + \frac{2}{3} = 0. \tag{20}$$

In summary, the three models described above assume t_c as a parameter proportional to the ratio of droplet size (D) and impact velocity (V) (Eq. 9 for Chandra *et al.* model and Eq. 18 for Pasandideh-Fard *et al.* and Mao *et al.* models) and the dissipation function ϕ defined by Eq. 7 to calculate W_{Diss}, therefore, increasing the uncertainty of the prediction. Moreover, while all these models are capable of predicting the D_m, they are only applicable to macroscopically smooth surfaces: Ra < 5 μm, which are far from those of skin (Ra = 50-200 μm). Previous models do not consider friction as

during droplet spreading, which is likely to be a dominant factor for *Ra* approaching those of skin, i.e., *Ra* > 50 μm. We suggest a new approach to evaluate W_{Diss}.

3. Analytical Model

From Eq. (14), the shear stress, τ, between the droplet and the impact surface during spreading can be expressed as

$$\tau = \eta \frac{\partial V_r}{\partial z} = \eta BrG''(0)\sqrt{\frac{B}{\nu}}, \tag{21}$$

where B is an undetermined constant and $G''(0)$ represents the wall shear stress, $G''(0) = 1.312$ [18]. Assuming axi-symmetric radial spreading, the differential friction force F between the droplet and the impact surface can be expressed as

$$dF = \tau\, dA = \eta BrG''(0)\sqrt{\frac{B}{\nu}} \cdot 2r\pi dr. \tag{22}$$

The overall energy dissipation, W_{Diss}, due to friction can be expressed as

$$dW_{Diss} = F \cdot dr. \tag{23}$$

Employing Eq. 22 and integrating both sides of Eq. (23) yields

$$W_{Diss} = \int_0^{\frac{D_m}{2}} \int_0^r \eta B\xi G''(0)\sqrt{\frac{B}{\nu}} \cdot 2\pi\xi d\xi dr = \frac{\pi}{96}\eta BG''(0)\sqrt{\frac{B}{\nu}} D_m^4. \tag{24}$$

Inserting W_{Diss} into Eq. (5) and re-arranging yields

$$\frac{G''(0)}{96}\frac{We}{\sqrt{Re}}\beta^5 D^{\frac{3}{2}} V^{-\frac{3}{2}} B^{\frac{3}{2}} + \frac{1}{4}(1-\cos\theta)\beta^3 - \left(\frac{We}{12}+1\right)\beta + \frac{2}{3} = 0. \tag{25}$$

In Eq. (25), all terms must be dimensionless, which again requires B to have dimensions of 1/sec. We propose

$$B = C_1 \frac{V}{D}, \tag{26}$$

where C_1 is an undetermined constant. This enables the product $D^{\frac{3}{2}} V^{-\frac{3}{2}} B^{\frac{3}{2}}$ within the 1st term in Eq. (25) to become a constant C. Simplifying Eq. (25):

$$\frac{CG''(0)}{96} \frac{We}{\sqrt{\mathrm{Re}}} \beta^5 + \frac{1}{4}(1-\cos\theta)\beta^3 - \left(\frac{We}{12}+1\right)\beta + \frac{2}{3} = 0. \tag{27}$$

4. Experimental Procedures

4.1 Droplet impact facilities

A schematic of our experimental setup is shown in Fig. 2. To minimize the evaporation of cryogen droplets during the experiments, the chamber was first pressurized to the saturation pressure of R-134a at room temperature (5.79 bar = 84 psi) using cryogen vapor. Then the pressure was increased slightly to 6.21 bar (90 psi) using pressurized air. After this, the chamber and droplet generator reservoir were cooled to approximately the same temperature (~ 5°C). Under these conditions, droplet spreading after impact can be considered isothermal without evaporation. It took more than 30 seconds for a droplet to evaporate completely after impact, which is at least three orders of magnitude higher than the time it takes a droplet to spread after impact (~2-8 ms).

The impact surfaces were horizontally mounted at the bottom of the chamber, and transparent windows made of polycarbonate were positioned on the two sides of the union to allow for side illumination and imaging. Pressure valves, gauges and safety instrumentation were mounted on the top cap of the PVC union.

Falling cryogen droplets were formed at the tip of small nozzles (3), which were attached to a needle valve (12) connected to a small cryogen tank (2) pressurized to (6.48 bar) (94 psi), which is slightly above the chamber's pressure. For proper comparison and analysis, it is necessary to maintain similarity between the smaller (3–20 μm) and faster (10–80 m/s) cryogen spray droplets and the larger and slower droplets we generate within the chamber. The average droplet size and velocities of the R134a spurts we have characterized in the past [8, 10] lead to ranges in Reynolds numbers (*Re*) of 200–9000 and Weber numbers (*We*) of 50–9000. Both of these dimensionless numbers are relevant to the physics of impact and spreading of liquids on solid surfaces [20]. By producing single droplets of R134a of 1.4-2.4 mm in diameter and 0.9–2.4 m/s in impact velocity, *Re* and *We* span from 9200-26500 and 258–1670, respectively. Note that the use of R134a is not only supported by the initial motivation of this study, but also because the viscosity and surface tension of R134a are about 5 times and 10 times lower than those of water, respectively, which allows us to overlap, at least partially, the ranges of *Re* and *We* of spray and single droplets.

The targeted flat surface was made of a mixture of 3100 epoxy resin and A210 Hardener (RBC Industries, Inc., Warwick, RI) with a ratio of 3:1 in weight. The mixture was poured into a Teflon mold with pre-sanded bottom that determines the surface roughness (*Ra*) of the targeted flat surface.

To fully scale the problem from the spray to the single droplet scenario, the surface roughness (*Ra*)—defined as half the distance between the average peak to valley separation of a rough surface [14]— would also need to be scaled. As mentioned above, *Ra* varies between 50 to 200 μm for human skin depending on the anatomical location,

age and race [14]. This means that the ratio of *Ra* of skin to a single spray droplet varies between 3 and 66, which would require the *Ra* of the human skin model to be 4–125 mm. However, *Ra* = 70 μm was set as the upper limit because splashing occurs beyond that roughness, so the continuity of the spread does no longer exist.

4.2 Imaging system

A high speed camera (Photron Fastcam PCI 10K, Itronics, Westlake Village, CA) with a 90 mm zoom lens (V-HQ Macro MC 90mm f/2.5, Elicar, Japan) was used to acquire digital images of single droplet impingement on the skin models. Image sequences were captured at a rate of 2000 frames per second with a pixel resolution of 128 × 64. Two Fiber-Lite illuminators (Edmund Industrial Optics, Barrington, NJ) were used as light sources, one in front and the other on the back of the chamber. To record droplet impingement dynamics, the camera was positioned at a 30^{o} angle with respect to the horizontal level. To clearly record the static contact angle, the camera was also mounted at the same level as the impingement surfaces. The droplet velocity was obtained using Motion software (Itronics, Westlake Village, CA) by comparing the same droplet in a series of consecutive frames. The velocity at which droplets break into smaller ones, or the breakup velocity, can be expressed as $V_b=\delta\sigma/C_d\rho D$ [21], where C_d is the drag coefficient. It was found that droplet impact velocity was far below the breakup velocity for the droplet sizes studied, which is the regime in which the model is applicable.

5. Results and Analysis

Figure 3 shows the time sequences of cryogen droplets with size D = 1.41 mm and V = 0.9 m/s impacting on flat surfaces with Ra = 0.5, 30 and 70 μm, respectively. The impact process can be divided into four continuous stages [21]. Stage 1: droplet spreads due to the kinetic energy before impact. Stage 2: the droplet spreads to the maximum diameter D_m and the kinetic energy is zero at this time. Stage 3: the spread droplet begins to retreat due to surface tension. Stage 4, the droplet either stays on the surface statically or rebounds.

These four stages can be clearly observed in the surface with Ra = 0.5 μm. The near perfect spherical cryogen droplet impinges onto the surface at t = 0.0 ms and spreads along the surface until reaching D_m at t = 8 ms. The droplet then begins to retreat, but at a much slower pace than it spreads. It takes about 70 ms (not shown) to reach Stage 4 where the droplet stays static at the surface.

For the surface with Ra = 30 μm, the impact dynamics exhibit some differences. Once the droplet impinges onto to the surface, it spreads as in the previous case, but at the same intervals of t = 1, 2 and 4 ms, the spread diameters are smaller than those of the surface with Ra = 0.5 μm. Also, the time required for the cryogen to spread to D_m is the same (8 ms), but after the cryogen reaches its D_m the retreat cannot be observed and the spread stays at almost the same position. For the surface with Ra = 70 μm, the impact dynamics are close to those of Ra = 30 μm.

Figure 4 shows spread diameter changes over time for different surface roughnesses Ra = 0.5, 4.2, 8.2, 30, 50 and 70 μm. For all surfaces, the time required for the cryogen to spread to D_m was approximately 8 ms. D_m decreases as Ra increases from

Ra = 0.5 μm to 70 μm. The surface with Ra = 0.5 μm displays a maximum spread distance D_m = 6.31 mm; however, as the surface roughness increases to Ra = 50 and 70 μm, D_m decreases to 4.9 mm and 4.6 mm, respectively. As pointed out above, once the cryogen spread reaches D_m, it begins to retreat for Ra = 0.5 μm, but for other Ra, the spread diameters remain unchanged with time.

Figure 5 shows the spread velocity variation with time for the six different surface roughnesses Ra = 0.5, 4.2, 8.2, 30, 50 and 70 μm. For all six surfaces, the spread velocities after impact decrease quickly within the first 4 ms, time after which the spread velocities reduce slowly to zero after D_m is reached (8 ms). The Ra also has an effect on the initial spread velocity, which is 1.7 1.4, 1.3, 1.1, 1.0 and 0.9 m/s for Ra = 0.5, 4.2, 8.2, 30, 50 and 70 μm, respectively.

Two more series of experiments with D = 1.91 mm and V = 2.38 m/s were performed. Table 1 shows a comparison of the normalized maximum spread diameter (β) for the three sets of experiments. For a droplet with D = 1.41 mm impacting a surface with Ra = 0.5 μm (Sets 1 and 2), β increases from 4.51 to 5.11 as V changes from 0.9 to 2.38 m/s. For the same V = 2.38 m/s (Sets 2 and 3), β also increases from 5.11 to 5.35 as D increases from 1.41 to 1.91 mm. Altering Ra to 50 and 70 μm results in a similar phenomena: increasing Ra causes a corresponding decrease in β for a given set of Re and We values.

The first term on the left hand side of Eq. (27) is the energy dissipation term which is the key factor influencing D_m. Figure 6 shows the effect of the undetermined coefficient C which appears in the first term of Eq. (27) on β. As C increases, β decreases for all three experimental sets, meaning that as the energy dissipation increases, the

maximum spread diameter must decrease. These results are also in agreement with previous research [19], which show that as *Ra* increases, the value of β decreases. Therefore, we used the following steps to associate *Ra* with the energy dissipation and to determine the value of *C* in the energy dissipation term of Eq. 27.

From Eq. (24), the energy dissipation term can be expressed as:

$$\frac{W_{Diss}}{\pi D^2 \sigma} = \frac{\frac{\pi}{96}\eta B G''(0)\sqrt{\frac{B}{\nu}} D_m^4}{\pi D^2 \sigma} \quad . \tag{28}$$

Inserting Eq. (26) into Eq. (28), and rearranging in terms of *Re* and *We*, we obtain

$$\frac{W_{Diss}}{\pi D^2 \sigma} = \frac{CG''(0)}{96} \frac{We}{\sqrt{\mathrm{Re}}} \beta^4 . \tag{29}$$

Considering a perturbation of the energy dissipation term, Eq. (29) can be written as

$$\frac{W_{Diss}}{\pi D^2 \sigma} = c \frac{We}{\sqrt{\mathrm{Re}}} \beta^4 (1+\varepsilon) , \tag{30}$$

where $c=CG''(0)/96$, and ε is a small perturbation which can be defined as:

$$\varepsilon = K_1 * \left(\frac{Ra}{D}\right)^{K_2} , \tag{31}$$

where K_1 and K_2 are constants that need to be found using experimental results. Inserting Eq. (31) into Eq. (27) we get

$$c \frac{We}{\sqrt{\mathrm{Re}}} (1 + K_1 * (\frac{Ra}{D})^{K_2}) \beta^5 + \frac{1}{4}(1-\cos\theta)\beta^3 - \left(\frac{We}{12}+1\right)\beta + \frac{2}{3} = 0 . \tag{32}$$

Note that if $Ra = 0$, Eq. (27) can be recovered.

The coefficients *c*, K_1 and K_2 of Eq. (32) were adjusted based on our experimental data using an iterative algorithm. Figure 7 shows the flowchart of this algorithm using experimental Set 1 as an example. Equation (32) has 5 solutions for β, however, only the

largest real root is considered, similar to Chandra *et al.* [15] procedure. By comparing the computed coefficients c, K_1 and K_2 for the three sets using the least squares method, only one set was found and the resulting equation for the prediction of β is:

$$0.0018 * \frac{We}{\sqrt{\mathrm{Re}}}(1 + 27.3 * (\frac{Ra}{D})^{0.76})\beta^5 + \frac{1}{4}(1 - \cos\theta)\beta^3 - \left(\frac{We}{12} + 1\right)\beta + \frac{2}{3} = 0 . \qquad (33)$$

To make sure the common solution set represents reasonably well all experimental cases, Figure 8 shows a comparison of the experimental data and the predictions by Eq. (33). The uncertainty of the experimental data is described using error bars, while the model predictions are expressed by continuous lines. For all cases, it is apparent that as the surface roughness Ra increases, β decreases and, as expected, the experimental and numerical results display consistency as the differences between them are less than 10%. Table 2 shows the predicted values of β by the three models described above plus the proposed model and the three sets of our experimental data. To further verify our model, we used two additional Plexiglas surfaces (Ra= 0.1 and 4.2 μm) and recorded the D_m resulting from 16 water droplets impacting under ambient pressure and temperature at ranges of Re =5,500 to 24,000 and We = 120-1330. A very good fit was found with confidence values within ± 10%.

Since the proposed model can be applied to surface roughnesses up to Ra= 70 μm, while the other three cannot, Ra was limited to 0.5 μm for this comparison. For Set 1, the experimental results and most model predictions are close. The notable exception is the model of Chandra *et al.* [15]. For Set 3, the predictions of the proposed model are also close to the experimental results, while the other models over predict β by at least 20%.

6. Discussion

The cryogen droplet impact monitored over identical time intervals shows that surface roughness affects maximum spread diameters (D_m). As Ra increases, D_m reduces dramatically, as seen in Figs. 3 and 4. This phenomenon can be best explained through principles of energy conservation: during the spread process, the larger the Ra, the larger the portion of energy consumed by friction between the cryogen droplet and impact surface. In Fig. 3, all droplets have the same D = 1.41 mm and V = 0.9 m/s. It follows that the kinetic energies prior to impact are the same. The energy dissipation during the spread process is greater for Ra = 30 μm than Ra = 0.5 μm. The energy lost influences the maximum spread diameter D_m. The droplet that dissipates more energy has less D_m. Therefore, for droplets with identical D and V values, increasing Ra of the impact surface will reduce D_m (or β).

Ra also affects the behavior after the liquid spreads to D_m. For the occurrence of the retreat phenomena, the surface energy should be large enough to overcome the energy consumed during the retreat process. Figure 3 shows pictures from spread to retreat after impact. It is obvious that the retreat phenomenon only occurs for Ra = 0.5 μm, but for Ra = 30 and 70 μm, this retreat phenomenon cannot be observed because the surface energy is not enough to overcome energy lost by friction during the spreading and is also insufficient to coalesce the droplet after D_m has been reached. Therefore, for surfaces with Ra = 50 and 70 μm, the cryogen droplet cannot retreat after spreading to D_m.

Also in Fig. 3, the geometry of the cryogen droplet spreads are different for various Ra. For Ra = 0.5 μm, the droplet remains together during impact, spreads and retreats. But for Ra = 30 and 70 μm, the droplet is separated into several parts after

spreading to D_m. This shows that increasing *Ra* can assist in breaking up liquid cryogen droplets. Because the resulting surface energy of a spread cryogen droplet is not enough to hold the cryogen together, the droplet breaks into several parts after reaching D_m and cannot retreat.

An important feature of the proposed model is that it directly associates *Ra* with energy dissipation during the spread process without the need of defining θ. In previous models designed to predict D_m, however, θ had to be measured for different *Ra*, although in all cases *Ra* was limited to < 5 μm. From Fig. 3, it is clear that for *Ra* = 30 and 70 μm, the measurement of θ becomes quite difficult because of the irregularity of the surface roughness, resulting in loss of accuracy. However, the average value of θ for the different surfaces used in this study is the same: $\theta = 15^o$, so only this constant value was used in our model. The effects of *Ra* on θ are subsequently and implicitly included in the first term of Eq. (33) because θ is a constant value for the same surface.

Figure 5 shows the spread velocity is also affected by *Ra*. The energy dissipation can also explain why the initial spread velocity changes with *Ra*. For droplets with the same size and impact velocity, the spread velocity should be the same without consideration of wall friction. For *Ra* = 0.5 μm, the spread velocity after 0.5 ms is 1.7 m/s, but for *Ra* = 70 μm, this value is only 0.9 m/s. This means that the energy dissipation caused by friction is much less for *Ra* = 0.5 μm than for *Ra* = 70 μm during the first 0.5 ms after impact. After t = 4.0 ms, the spreading velocities are almost the same for all *Ra*, suggesting that most of the energy dissipation occurs during the first half of the spreading process.

Our results support the concept of a constant characteristic time t_c, representing the time from impact to maximum spread, D_m. In previous models, this time was defined as D/V [15] or $\frac{8}{3}D/V$ [17, 19] and was used to find the energy dissipation (W_{diss}). While our proposed model does not need an explicit definition of t_c, we can observe from our experimental results that t_c is essentially equal to 8.0 ms (Figs. 4 and 5), while the definitions of D/V and $\frac{8}{3}D/V$ result in shorter times (e.g., 0.8 and 2.1, respectively, for Set 3). Consequently, the corresponding W_{diss} in previous models is likely underestimated.

It is also noteworthy that while t_c might be a constant, the spreading velocity and, consequently, the instantaneous W_{diss} are not. Fig. 5 shows that the spreading velocity shortly after impact and up to about 4.0 ms is significantly higher for the smooth surfaces, but its rate of decrease is larger. After 4.0 ms, the spread velocity is the same for all surfaces. That is, the larger *Ra* is, the more significant the loss of kinetic energy is for the thin-spreading layer that exists during the first 4.0 ms and, consequently, the velocity drop in that initial period is large relative to the one after 4.0 ms (Fig. 5). Since the energy dissipation after 4.0 ms is less, the spread velocity remains nearly constant and below 0.2 m/s, independent of *Ra*. Note that the spread velocities for all *Ra* are close to zero after 8.0 ms when the spread reaches the maximum value (D_m).

Figure 9 shows the comparison of β computed by the four models for Ra = 0.5 μm as a function of *We*. For *We* = 258 (minimum value), all model predictions are close to the experimental results, except for *We* = 1680 (maximum value), where the error of some other models can be as large a twofold. Therefore, is appears that models that do

not consider friction loss during the spread process may be accurate for predicting D_m for small droplets at low impact velocity (low *Re* and *We*), but lose accuracy for large droplets with high impact velocity (high *Re* and *We*).

Figure 10 shows the comparison of experimental results from four other sources according to Table 3 with the predicted β by the proposed model. Note that the present model is more accurate for droplets with higher impact velocity. For Prunet-Foch *et al.* [22] experimental results, the droplets have the same impact velocity $V = 3.5$ m/s but with different surface roughness. The errors between the calculated β using the present model and the experimental data are only 5%.

For Mao *et al.* [19] experimental results, the proposed model is reliable for $V > 1.86$ m/s, but looses its accuracy for $V < 1$ m/s. This can also be observed using Rioboo's *et al.* [23] experimental results. With $V = 3.6$ m/s, the errors between measured and calculated β are 10 %. However, with impact velocity of 1.18 m/s, the error increases. For Moita *et al.* [24] experiments, the proposed model cannot predict the correct results for droplets with $V = 0.44$ m/s.

In summary, increasing the droplet velocity or *Ra* makes friction effects on D_m more prominent. The spread velocity increases with increasing droplet impact velocity [21], but the effect of *R*a is more prominent as the spread velocity increases. Therefore, the proposed model is more accurate predicting D_m for droplets with large impact velocity (1.86–3.72 m/s) impacting on surfaces with a wide range of roughnesses (0.5–70 μm).

One of the most significant advantages of presented model is that the effect of *Ra* on D_m is directly and explicitly associated with the surface roughness. Thus the errors

caused by estimating t_c could be reduced. Even though the scales between CSC of human skin and our experimental set up are not comparable, our study shows how droplet spread varies as a function of *Ra* and the effect of *Ra* on spread dynamics. In addition, we used our experimental results to build on existing models of maximum spreading by accounting for surface roughness during energy dissipation. To the best of our knowledge, this is the first study that considers surface roughness as a free parameter. Knowing the effect of surface roughness on liquid spread may enable engineers to appropriately modify either liquid or substrate properties to enhance many applications, e.g., addition of surfactants to sprays, peeling of the stratum corneum for improved skin cooling or moisturizer penetration.

7. Conclusion

Both the experimental and modeling results demonstrate that the surface roughness *Ra* affects the cryogen impact and spreading dynamics. For a droplet with the same size and velocity, the smaller the impact surface roughness *Ra*, the larger the spread diameter D_m. For impact surfaces with *Ra* greater than 30 μm, the cryogen retreat phenomenon cannot be observed. The proposed model appears to predict D_m for surfaces with large *Ra*, like human skin, better than previous models because it considers the effect of friction loss due to surface roughness and reduces the uncertainty of defining a spread time t_c. The comparison of the experimental and modeling results demonstrates the accuracy of this model to predict the maximum spread diameter (D_m) of droplet impingement onto surfaces with a large range of surface roughnesses (*Ra*).

Acknowledgements

This work has been supported in part by NIH Grant (K01-42057) and the UCR Academic Senate Grant 05-06. The authors also thank Dr. Wangcun Jia at University of California, Irvine for helpful discussions.

Nomenclature

C_d	drag coefficient
D	droplet diameter [mm]
D_m	maximum spread diameter [mm]
g	gravity [m s^2]
G	similarity function
h	thickness of flatten cryogen at maximum spread diameter [mm]
r	radius of cryogen spread [mm]
Ra	surface roughness [μm]
Re	Reynolds number ($\rho VD/\eta$)
t	time [ms]
t_c	characteristic spread time [ms]
T	temperature [^{o}C]
T_{sat}	saturation temperature of cryogen at 1 bar [^{o}C]
V	droplet velocity [m/s]
V_b	droplet breakup velocity [m/s]
V_r	velocity along radial direction [m/s]
V_Z	velocity along vertical direction [m/s]
W_{Diss}	energy dissipated during cryogen spread [m s]
We	Weber number ($D\rho V^2/\sigma$)

Greek symbol

α	similarity variable
β	D_m/D (ratio of the maximum spread diameter over droplet diameter)
δ	boundary layer thickness [mm]
η	dynamic viscosity [N s/$m^{2]}$
ϕ	dissipation function [N/m s]
ν	kinetic viscosity [m^2/s]
θ	static wetting angle [^{o}]
ρ	density [kg/m^3]
σ	surface tension [N/m]
σ_{LV}	surface tension between liquid and vapor [N/m]
σ_{SL}	surface tension between liquid and solid surface [N/m]
σ_{SV}	surface tension between vapor and solid surface [N/m]

τ	shear stress [N/m^2]
ψ	stream function

References

1. KM Kelly, JS Nelson, GP Lask, RG Geronemus, LJ Bernstein, *Cryogen spray cooling in combination with nonablative laser treatment of facial rhytides*. Archives of Dermatology. Vol. 135. 1999. 691-694.
2. JS Nelson, TE Milner, B Anvari, BS Tanenbaum, S Kimel, LO Svaasand, SL Jacques, *Dynamic epidermal cooling during pulse-laser treatment of port-wine stain-A new methodology with preliminary clinical evaluation*, in *Achives of Dermatology*. 1995. p. 695-700.
3. MP Goldman, RE Fitzpatrick. *Cutaneous Laser Surgery*. 1999. Chicago: Mosby.
4. JS Nelson, TE Milner, B Anvari, BS Tanenbaum, S Kimel, LO Svaasand, SL Jacques, *Selective photothermolysis and removal of cutaneous vasculopthies and tattoos by pulsed laser*, in *Plastic and Reconstructive Surgery*. 1991. p. 723-731.
5. B Anvari, TE Milner, BS Tanenbaum, S Kimel, LO Svaasand, JS Nelson, *Dynamic epidermal cooling in conjunction with laser treatment of port-wine stains: Theoretical and preliminary clinical evaluations*, in *Laser in Medical Science*. 1995. p. 105-112.
6. G Aguilar, B Majaron, K Pope, LO Svaasand, EJ Lavernia, JS Nelson, *Influence of nozzle-to-skin distance in cryogen spray cooling for dermatologic laser surgery*, in *Lasers in Surgery and Medicine*. 2001. p. 113-120.
7. G Aguilar, H Vu, JS Nelson, *Influence of angle between the nozzle and skin surface on the heat flux and overall heat extraction during cryogen spray cooling*, in *Physics in Medicine and Biology*. 2004. p. N147-N153.
8. G Aguilar, B Majaron, W Verkruysse, Y Zhou, JS Nelson, EJ Lavernia, eds. *Theoretical and experimental analysis of droplet diameter, temperature, and evaporation rate evolution in cryogenic sprays*. International Journal of Heat and Mass Transfer. Vol. 44. 2001. 3201-3211.
9. G Aguilar, B Majaron, E Karapetian, EJ Lavernia, JS Nelson, *Experimental study of cryogen spray properties for application in dermatologic laser surgery*, in *IEEE Transactions on Biomedical Engineering*. 2003. p. 863-869.
10. W Franco, H Vu, W Jia, JS Nelson, G Aguilar, *Fluid and thermal dynamics of cryogen sprays impinging on a human tissue phantom*, in *In progress*. 2007.
11. G Aguilar, GX Wang, JS Nelson, *Dynamic behavior of cryogen spray cooling: Effects of spurt duration and spray distance*, in *Lasers in Surgery and Medicine*. 2003. p. 152-159.
12. K Gasljevic, G Aguilar, EF Matthys, *On two distinct types of drag-reducing fluids, diameter scaling, and turbulent profiles.* Journal of Non-Newtonian Fluid Mechanics, 2001. **96**(3): p. 405-425.
13. JW Tunnell, JH Torres, B Anvari, *Methodology for estimation of time-dependent surface heat flux due to cryogen spray cooling*, in *Annals of Biomedical Engineering*. 2002. p. 19-33.

14. W Manuskiatti, DA Schwindt, HI Maibach, *Influence of age, anatomic site and race on skin roughness and scaliness*, in *Clinical and Laboratory Investigations*. 1998. p. 401-407.
15. S Chandra, CT Avedisian, *On the Collision of a Droplet with a Solid-Surface*, in *Proceedings of the Royal Society of London Series a-Mathematical Physical and Engineering Sciences*. 1991. p. 13-41.
16. A Frohn, N Roth, *Dynamics of Droplets*. 2000, Springer: New York.
17. M Pasandideh-Fard, YM Qiao, S Chandra, J Mostaghimi, *Capillary effects during droplet impact on a solid surface*, in *Physics of Fluids*. 1996. p. 650-659.
18. FM White, *Viscous Fluid Flow*. 1991, McGrawHill: New York.
19. T Mao, D Kuhn, *Spread and rebound of liquid droplets upon impact on flat surfaces*, in *AICHE*. 1997. p. 2169-2179.
20. EJ Lavernia, Y Wu, *Spray atomization and deposition*. 1996, John Wiley: New York.
21. M Rein, *Phenomena of liquid drop impact on solid and liquid surface*, in *Fluid Dynamics Research*. 1993. p. 61-93.
22. B Prunet-Foch, F Legay, M Vignes-Adler, C Delmotte, *Impacting Emulsion Drop on a Steel Plate: Influence of the Solid Substrate*, in *Journal of Colloid and Interface Science*. 1998. p. 151-168.
23. R Rioboo, M Marengo, C Tropea, *Time evolution of liquid drop impact onto solid, dry surfaces*, in *Experiments in Fluids*. 2002. p. 112-124.
24. A Moita, A Moreira, *Influence of surface properties on dyanmic behavior of impacting droplet*, in *9th International Conference on Liquid Atomization and Spray System*. 2003: Sorrento, Italy.

TABLES

Droplet parameters	Surface roughness Ra (μm)	β
Set 1: Re = 9200	0.5	4.51
We = 258	4.2	4.23
D = 1.41 mm	8.2	4.02
V = 0.9 m/s	30	3.74
	50	3.52
	70	3.26
Set 2: Re = 20000	0.5	5.11
We = 1210	4.2	4.78
D = 1.41 mm	8.2	4.69
V = 2.38 m/s	30	4.1
	50	3.81
	70	3.58
Set 3: Re = 26500	0.5	5.35
We = 1670	4.2	4.95
D = 1.91 mm	8.2	4.78
V = 2.38 m/s	30	4.4
	50	4.12
	70	3.9

Table 1. Three experimental cases and results.

	Set 1 D = 1.41 mm V = 0.9 m/s β	**Set 2** D = 1.41 mm V = 2.38 m/s β	**Set 3** D = 1.91 mm V = 2.38 m/s β
Chandra *et al.* [15]	6.45	6.95	8.82
Pasandideh-Fard *et al.* [17]	4.83	5.97	6.43
Mao's *et al.* [19]	4.68	5.42	6.40
Liu *et al.* proposed model	4.61	5.0	5.20
Experimental data (Eq. 33)	4.51	5.11	5.35

Table 2. Comparison of four models using present experimental results for Ra = 0.5 μm

Diameter (mm)	*Velocity (m/s)*	*Re*	*We*	*Ra (μm)*	*θ*	*Measured* β	*Calculated* β		*Ref.*
2.7	3.5	9000	960	0.5	40	4.2	4.4	○	[22]
2.7	3.5	9000	960	2	15	3.9	4.1	○	[22]
2.7	3.5	9000	960	5	30	3.7	3.9	○	[22]
2.7	3.5	9000	960	0.5	55	4.1	4	○	[22]
2.7	3.5	9000	960	2	35	3.8	4.1	○	[22]
2.7	0.55	1485	12	5	97	1.65	2.2	△	[19]
2.7	0.82	2214	25	5	97	2.1	2.6	△	[19]
2.7	1	2700	37	5	97	2.26	2.8	△	[19]
2.7	1.58	4266	92	5	97	3.1	3.2	△	[19]
2.7	1.86	5022	127	5	97	3.6	3.5	△	[19]
2.7	2.77	7480	282	5	97	4.32	3.8	△	[19]
2.7	3.72	10044	509	5	97	4.78	4.3	△	[19]
2.7	0.55	1485	12	0.5	67	1.67	2.8	△	[19]
2.7	0.82	2214	25	0.5	67	2.16	3.3	△	[19]
2.7	1	2700	37	0.5	67	2.34	3.5	△	[19]
2.7	1.58	4266	92	0.5	67	3.09	3.6	△	[19]
2.7	1.86	5022	127	0.5	67	3.67	4.1	△	[19]
2.7	2.77	7480	282	0.5	67	4.42	4.4	△	[19]
2.7	3.72	10044	509	0.5	67	4.88	4.6	△	[19]
2.7	0.55	1485	12	0.2	37	1.77	3.2	△	[19]
2.7	0.82	2214	25	0.2	37	2.2	3.6	△	[19]
2.7	1	2700	37	0.2	37	2.53	3.7	△	[19]
2.7	1.58	4266	92	0.2	37	3.11	4	△	[19]
2.7	1.86	5022	127	0.2	37	3.7	4.1	△	[19]
2.7	2.77	7480	282	0.2	37	4.5	4.7	△	[19]
2.7	3.72	10044	509	0.2	37	4.94	4.9	△	[19]
3.04	1.18	3587	58	0.003	10	3.2	5.1	△	[19]
3.17	3.6	11412	563	0.003	10	5.3	5.7	▽	[23]
3.03	1.18	3587	58	3.6	78	2.6	3.7	▽	[23]
3.17	3.6	11412	563	3.6	78	4.6	4.3	▽	[23]
3.03	1.18	3587	52	0.4	105	2.4	2.7	▽	[23]
3.17	3.6	11412	563	0.4	105	5	4.7	▽	[23]
3	1.18	3587	57	25.6	105	2.5	2.7	▽	[23]
3.17	3.6	11412	563	25.6	105	4.9	4.2	▽	[23]
2.65	1.22	3233	54	6.2	100	2.6	3.02	▽	[23]
3.42	3.62	12380	614	6.2	100	5	4.3	▽	[23]
2.65	1.22	3233	54	6.2	90	2.6	3.1	▽	[23]
3.52	3.62	12380	614	6.2	90	5.1	4.3	▽	[23]
3.2	0.44	1408	452	2	85	1.4	3.5	◇	[24]
3.2	0.44	1408	452	2.7	85	1.4	3.33	◇	[24]
3.2	0.44	1408	452	1.52	71	1.5	3.3	◇	[24]
3.2	0.44	1408	452	3	86	1.4	3.3	◇	[24]

Table 3. Comparison of calculated β using our proposed model with experimental results from previous works.

FIGURES

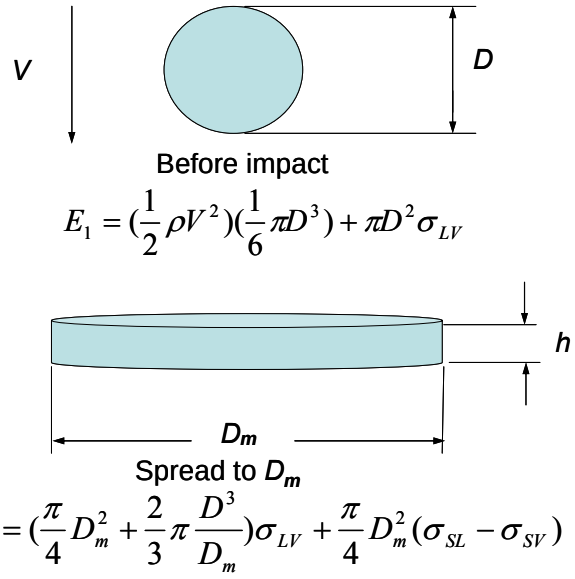

Figure 1. Sketch of shape and energy of droplet before impact and at maximum spread diameter D_m.

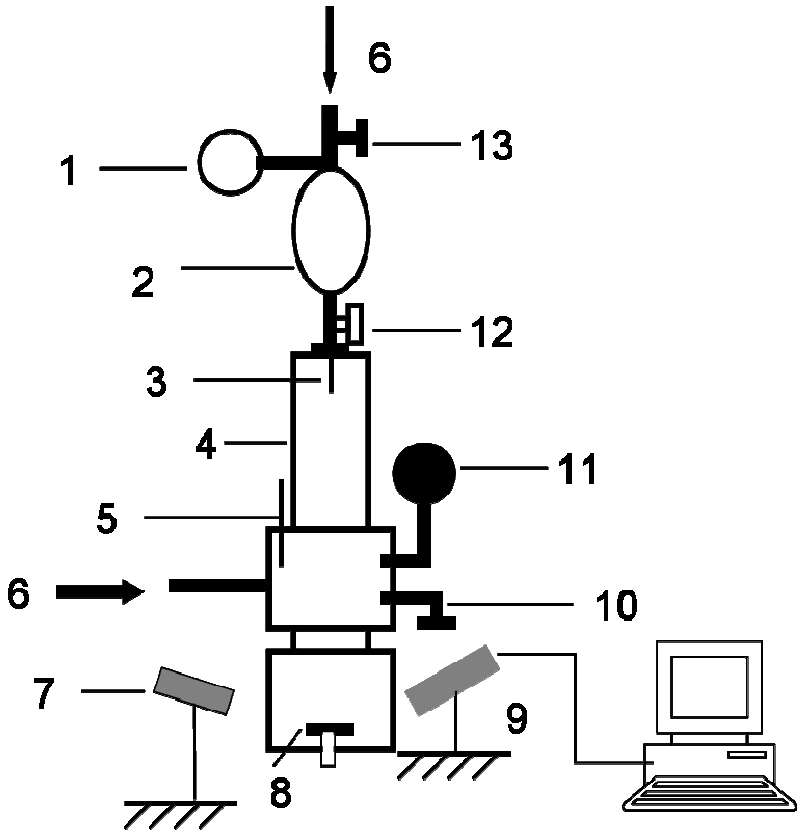

Figure 2. Experimental facilities for experiments of cryogen droplet impact dynamics without evaporation. 1. Pressure gauge; 2. Cryogen tank; 3. Nozzle; 4. Clear PVC tower; 5. Temperature sensor; 6. Pressured gas; 7. Illumination; 8. Impact surface; 9. High speed camera; 10. Pressure relieve valve; 11. Pressure gauge; 12. Needle valve; 13. Ball valve.

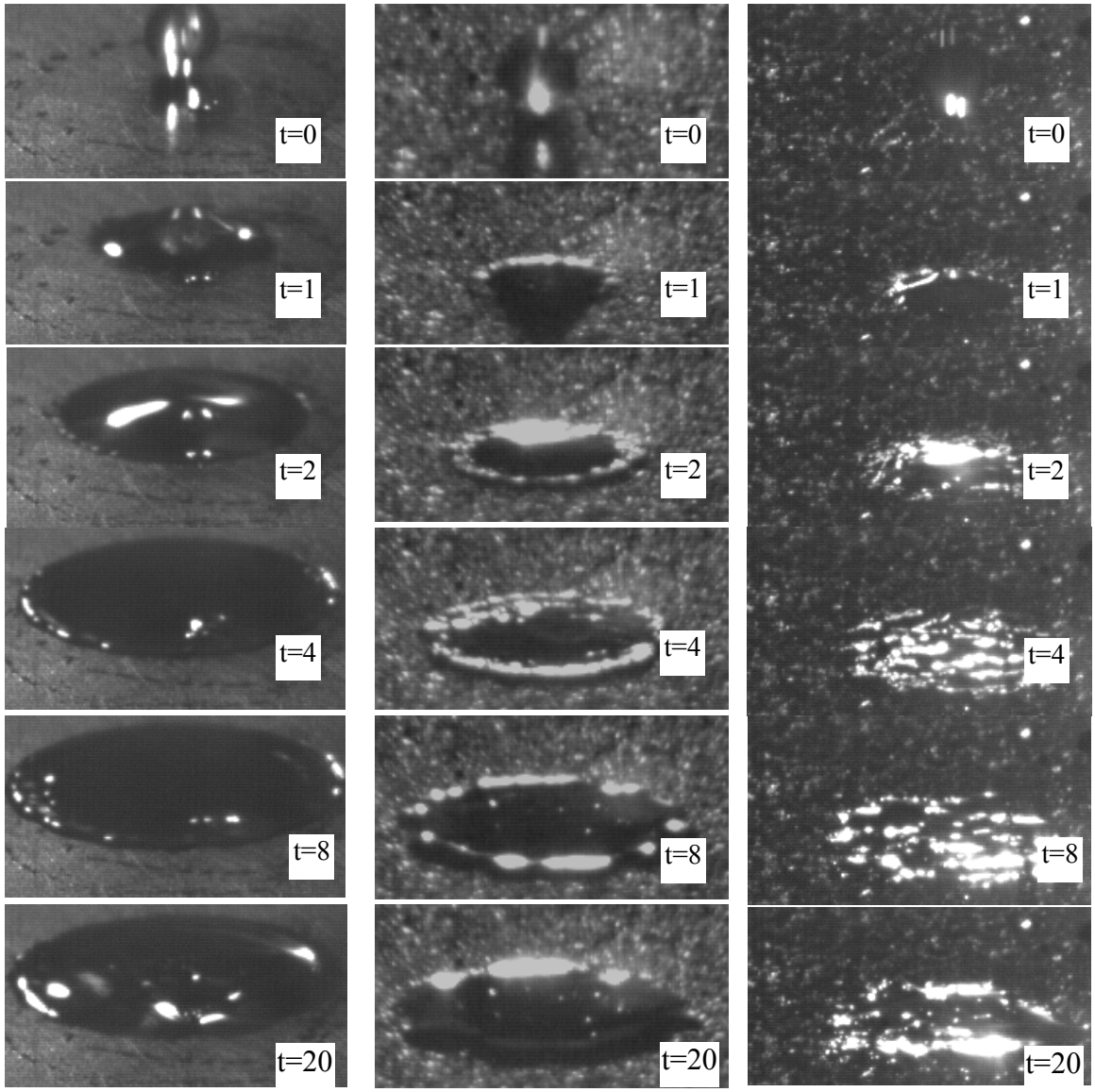

Figure 3. Droplet with D = 1.41 mm and V = 0.9 m/s, Re = 9200 and We = 258 impact onto three surfaces with Ra = 0.5 μm (left), Ra = 30 μm (middle) and Ra = 70 μm (right) for various times ranging from 0-20 ms.

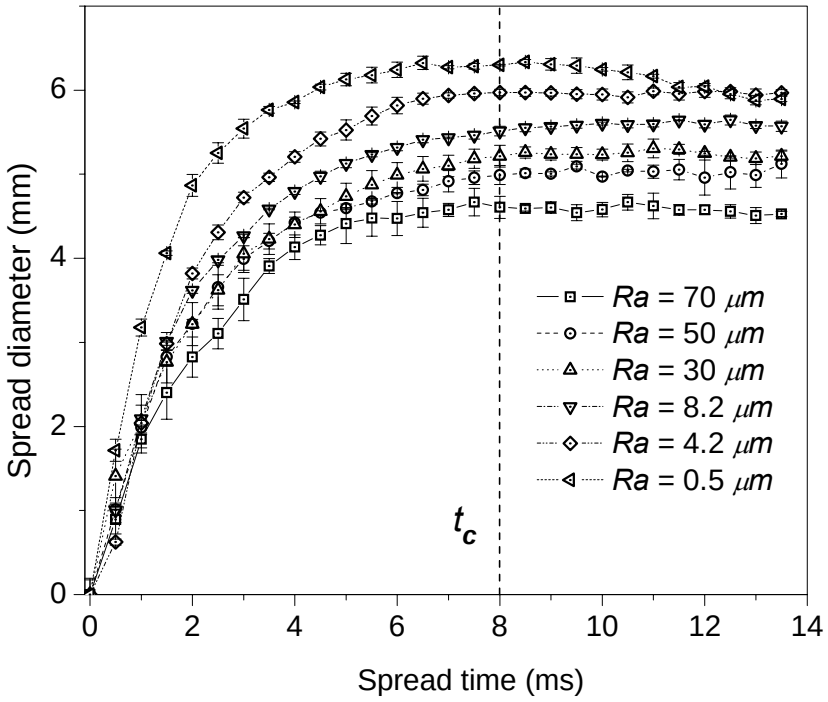

Figure 4. Spread diameter vs. spread time for surface roughness Ra = 0.5 ,4.2, 8.2, 30, 50 and 70 μm, respectively, with droplet with D = 1.41 mm and V = 0.9 m/s.

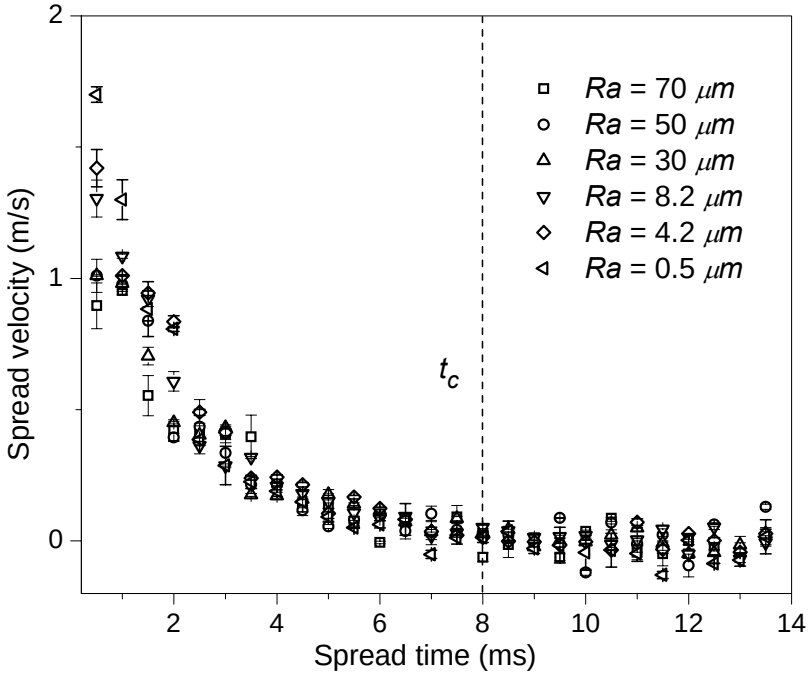

Figure 5. Spread velocity vs. spread time for surface roughness Ra = 0.5 ,4.2, 8.2, 30, 50 and 70 μm, respectively, with droplet with D = 1.41 mm and V = 0.9 m/s.

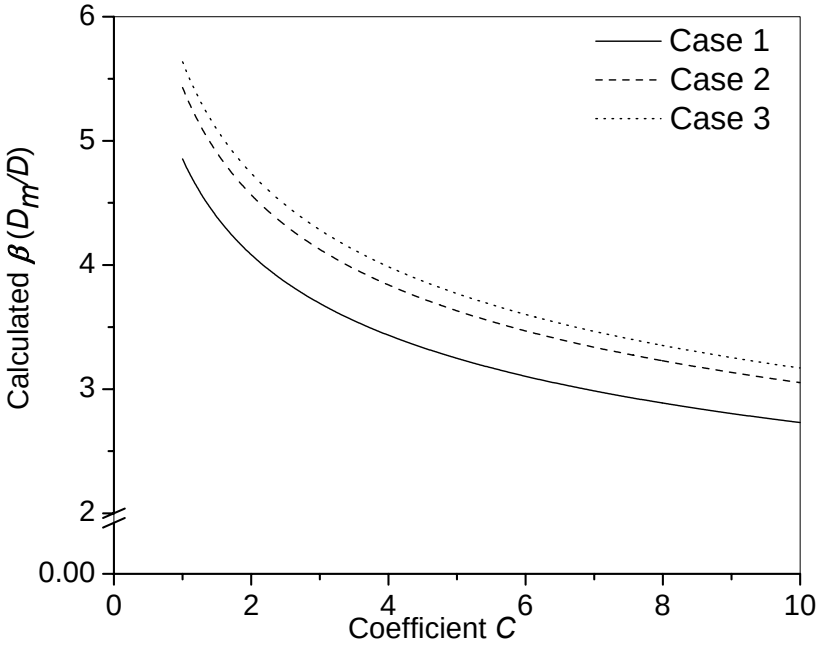

Figure 6. Prediction of β with undetermined coefficient C in Eq. 27:
Case 1: D = 1.41 mm and V = 0.9 m/s, Re = 9200 and We = 258;
Case 2: D = 1.41 mm and V = 2.38 m/s, Re = 20000 and We = 1210;
Case 3: D = 1.91 mm and V = 2.38 m/s, Re = 26500 and We = 1670.

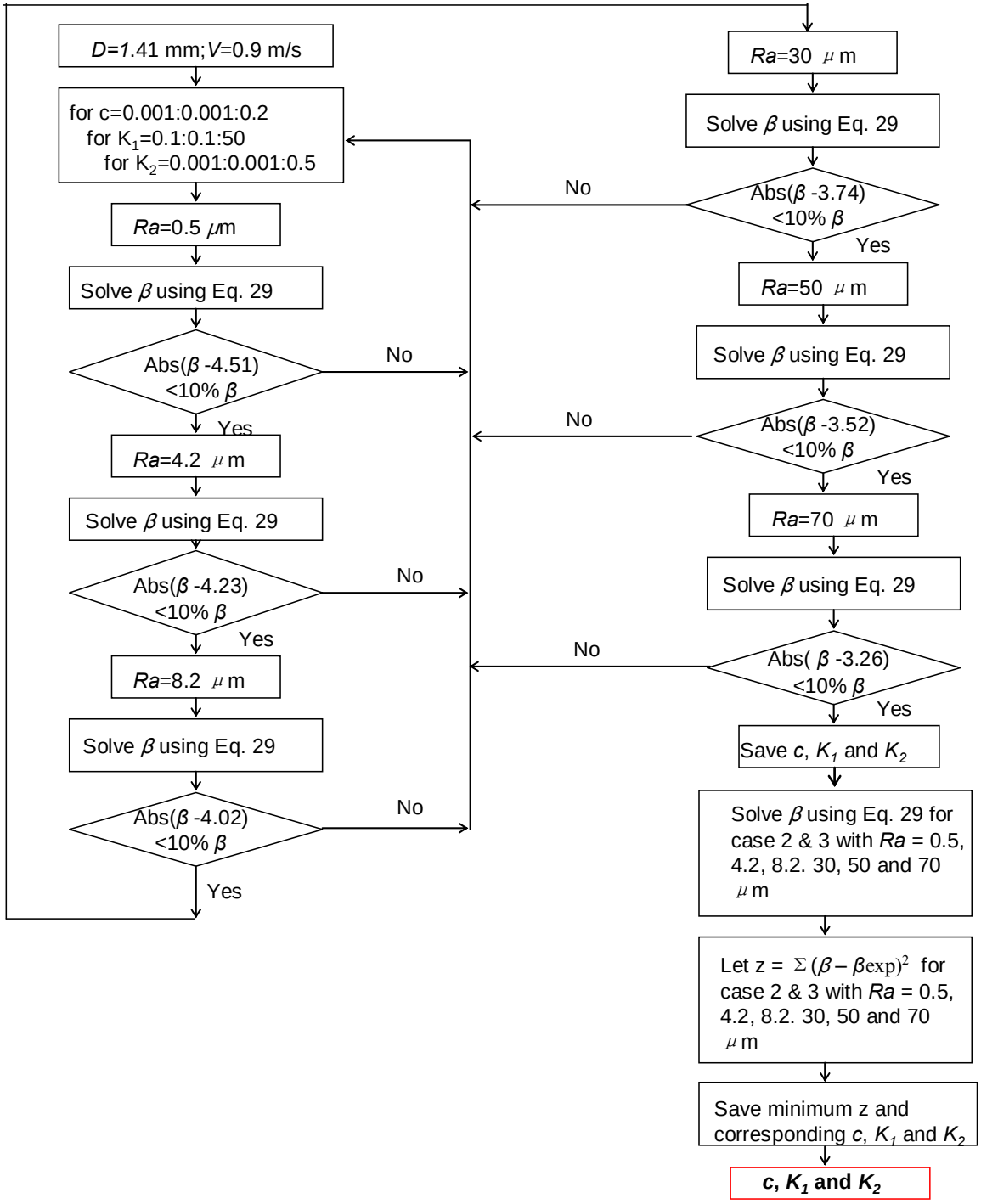

Figure 7. Flowchart of algorithm to determine the coefficients c, K_1 and K_2 for experiment results.

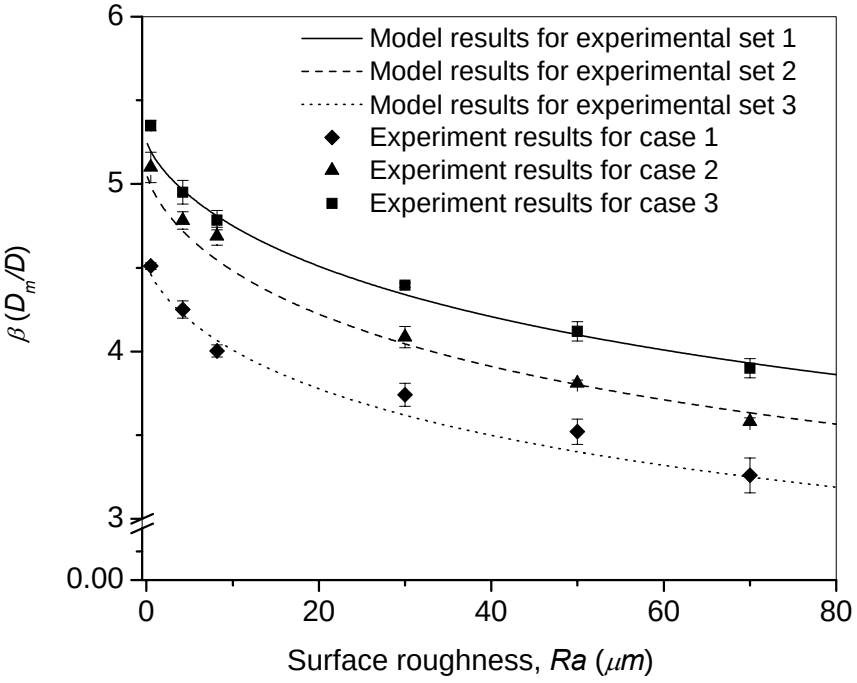

Figure 8. Experimental and model predicted results of β for three cases:
Case 1: D = 1.41 mm and V = 0.9 m/s, Re = 9200 and We = 258;
Case 2: D = 1.41 mm and V = 2.38 m/s, Re = 20000 and We = 1210;
Case 3: D = 1.91 mm and V = 2.38 m/s, Re = 26500 and We = 1670.

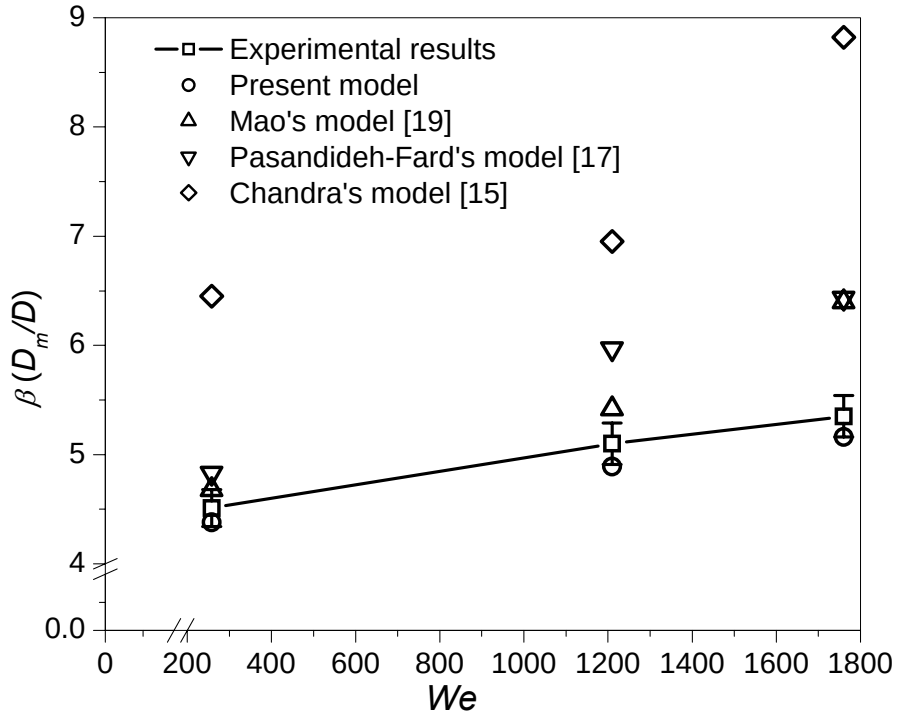

Figure 9. Comparison of our experimental results with previous models [15, 17, 19] for the same three cases described in Table 2 with Ra = 0.5 μm.

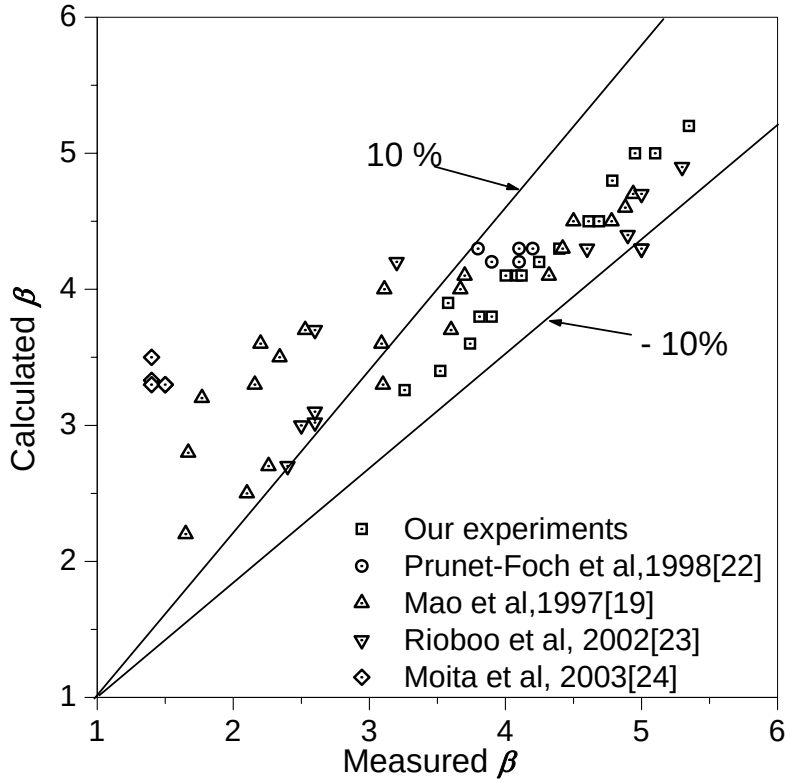

Figure 10. Comparison of the β using the present model with experimental data from current and previous work [20, 22, 23, 24].